Supporting information

$FeCl_3$-functionalized graphene oxide/single-wall carbon nanotube/silicon heterojunction solar cells with an efficiency of 17.5%

Xian-Gang Hu[a,b], Qinwei Wei[a,b], Yi-Ming Zhao[a,b], Peng-Xiang Hou[a,b,*], Wencai Ren[a,b], Chang Liu[a,b,*], Hui-Ming Cheng[a,c]

[a] *Shenyang National Laboratory for Materials Science, Institute of Metal Research, Chinese Academy of Sciences, Shenyang 110016, PR China.*

[b] *School of Materials Science and Engineering, University of Science and Technology of China, Shenyang, 110016, PR China.*

[c] *Shenzhen Geim Graphene Center, Shenzhen International Graduate School, Tsinghua University, Shenzhen 518055, PR China*

Corresponding Authors: pxhou@imr.ac.cn; cliu@imr.ac.cn

Experimental Section

Preparation of SWCNT films and the GO, $FeCl_3$ solutions. The SWCNT films were synthesized by a FCCVD method[1, 2]. Ethylene and hydrogen were used as the carbon source and carrier gas, respectively. A mixed solution containing toluene, ferrocene and thiophene was used as the respective liquid carbon source, catalyst precursor and growth promoter, and was injected into a quartz tube reactor by a syringe pump. The growth temperature was 1100℃. The SWCNT film was collected on a membrane filter (0.45 μm pore diameter) at room temperature and could be easily transferred onto a target substrate, as reported previously[2]. The GO sheets were synthesized by the water electrolytic oxidation of graphite dispersed in water[3], which was then diluted with ethanol to a concentration of 0.25 mg mL^{-1}. The $FeCl_3$ solution was prepared by adding $FeCl_3 \cdot (H_2O)_6$ to ethanol with a concentration of 3.6 mg mL^{-1} .

Fabrication of heterojunction solar cells. A n-type silicon wafer (2-4 Ω cm) covered with a 300 nm-thick layer of thermal silicon oxide was patterned with a square window (3 mm×3 mm), and the silicon oxide in the square area was then etched away by a buffered oxide etchant (6:1 of 40% NH_4F and 49% HF) and rinsed with water and isopropanol to form the active area (~0.09 cm^2). The SWCNT film was transferred onto the top surface of the Si substrate to fabricate the SWCNT/Si heterojunction. Silver paste was painted around the active area to serve as a front electrode, while the back electrode was a gallium-indium eutectic, which formed ohmic contact with the silicon. A $FeCl_3$-GO-SWCNT/Si solar cell was fabricated by drop-coating GO and $FeCl_3$ solutions onto the surface of a SWCNT/Si solar cell.

Characterization. Raman spectra of the films were obtained using a Jobin-Yvon Labram HR800 instrument, excited by a 633 nm laser. Raman mapping was achieved using a WITec alpha300 instument. XPS and UPS were measured using an Esclab-250 instrument. The optical transmission and absorption spectra of the films and the reflectance of the solar cells were measured using an UV–Vis–NIR spectrophotometer (AGILENT CARY 5000) equipped with an integration sphere. The structure of the films was characterized by SEM (Nova Nano SEM 430) and TEM (Tecnai F20, operated at 200 kV). The film thickness was measured by a step profiler. The I-V curves of the films were measured by a source meter (Keithley 2450). Solar cell characteristics were determined by a solar simulator (PEC-L01 from Peccell Technologies, Inc.) under AM 1.5 G (100 mW/cm^2) light and a source meter (Keithley 2450). The J-V curves were measured by using a reverse scan (from 1 V to -1 V) with a step voltage of 10 mV. The irradiation intensity was calibrated using a standard Si solar cell (PECSI 02). EIS measurements of the solar cell were made in the frequency range 10 Hz to 1 MHz at room temperature by an electrochemical workstation (BioLogic VSP-300).

Figure S1. Optical image of the GO dispersion in a mixture of deionized water and ethanol (0.25 mg/ml).

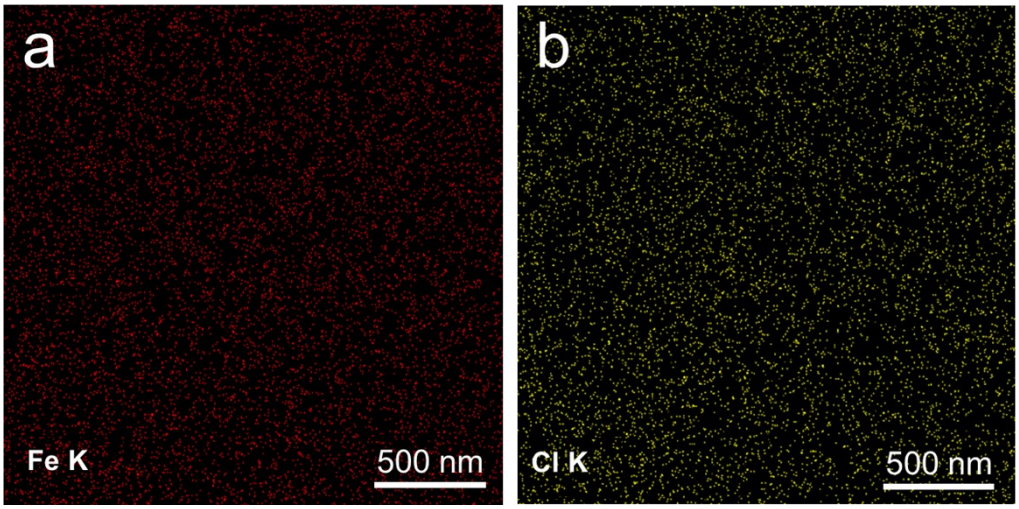

Figure S2 Elemental distribution analysis of the (a) Fe and (b) Cl for the $FeCl_3$-GO-SWCNT film.

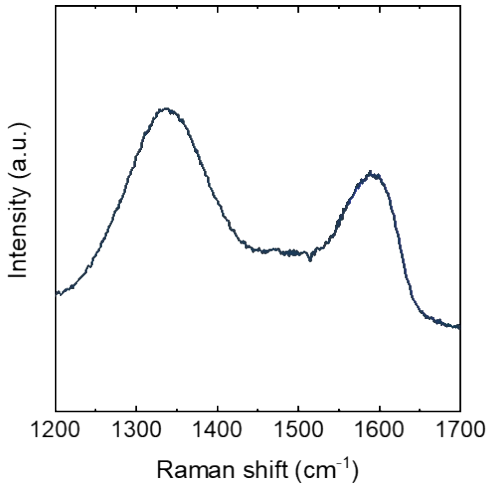

Figure S3. Laser Raman spectrum of the GO film.

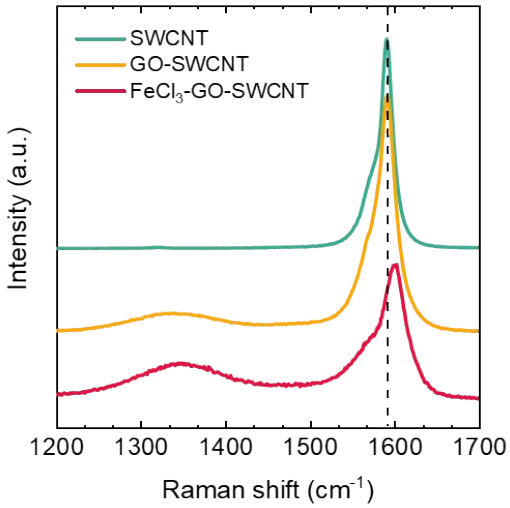

Figure S4. Laser Raman spectra of the SWCNT, GO-SWCNT and $FeCl_3$-GO-SWCNT films.

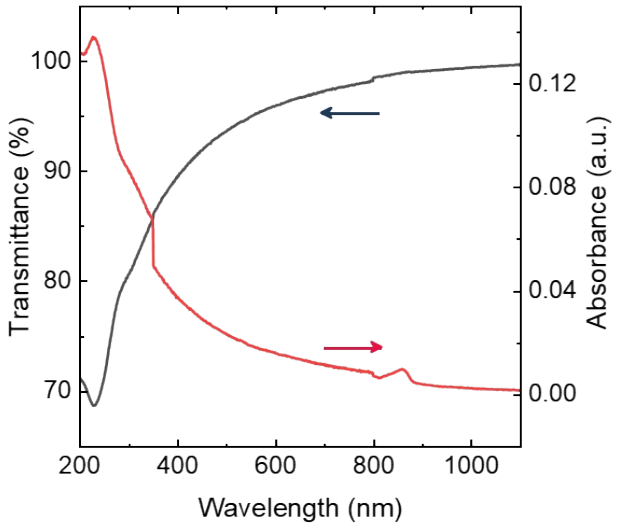

Figure S5. Optical transmittance and absorbance of the GO film.

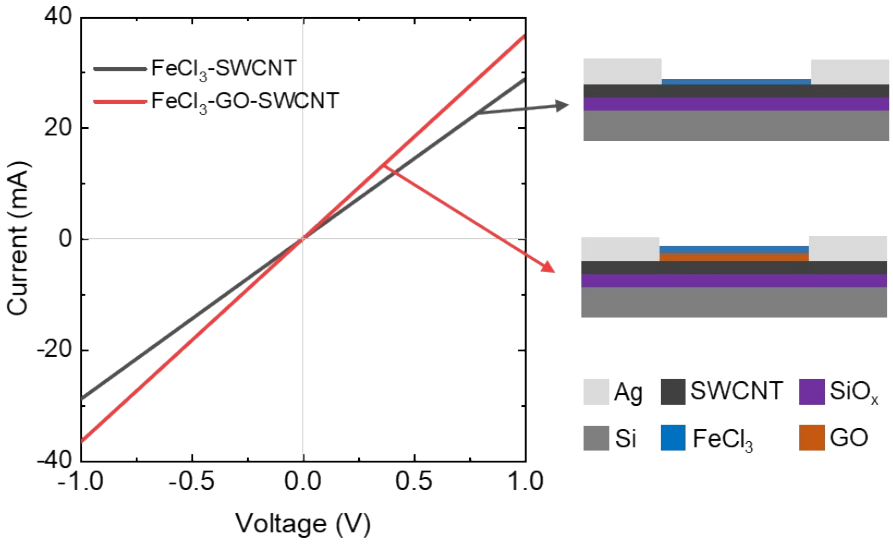

Figure S6. I-V curves of the $FeCl_3$-GO film and $FeCl_3$-GO-SWCNT films

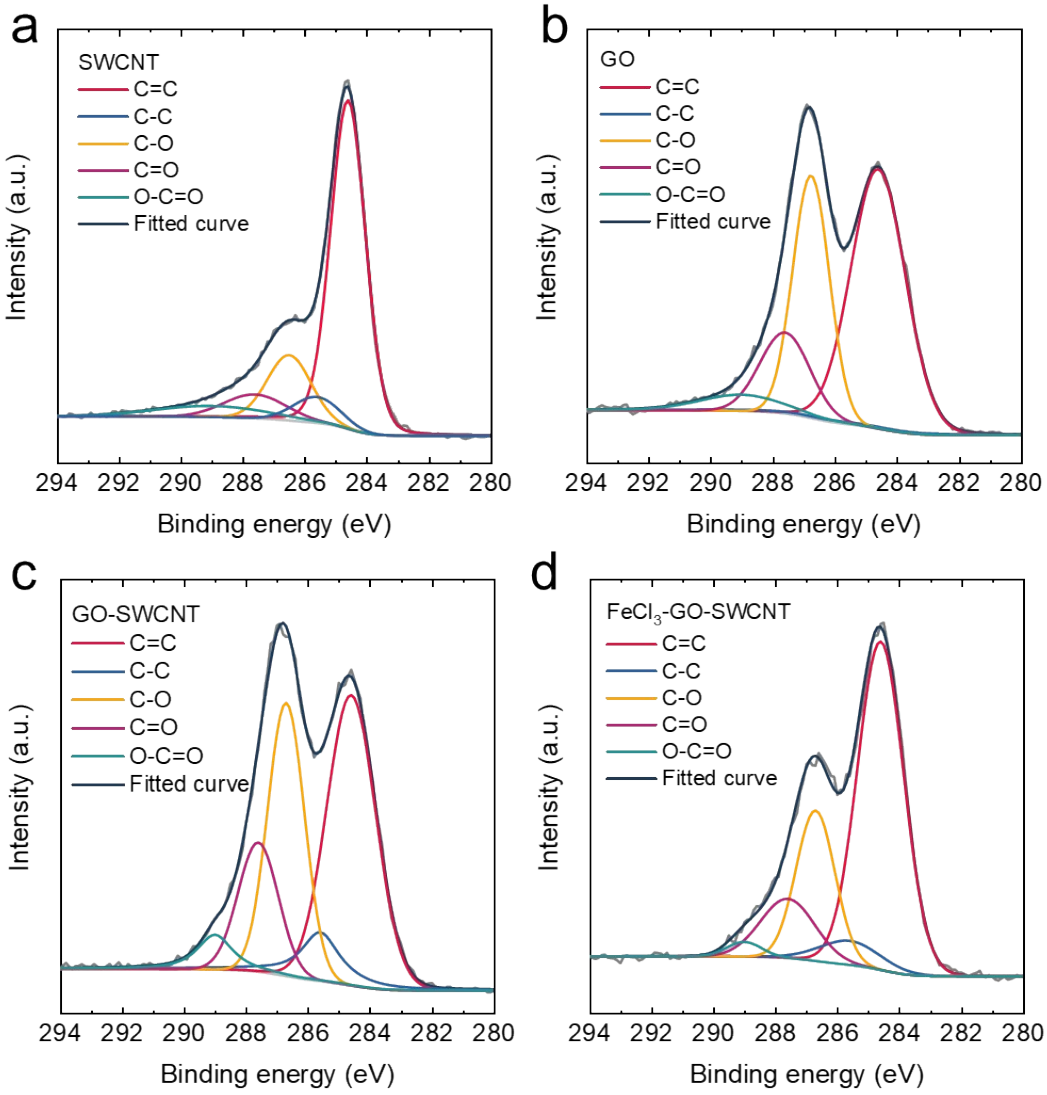

Figure S7. C1s spectra of (a) SWCNT, (b) GO, (c) GO-SWCNT, and (d) $FeCl_3$-GO-SWCNT films.

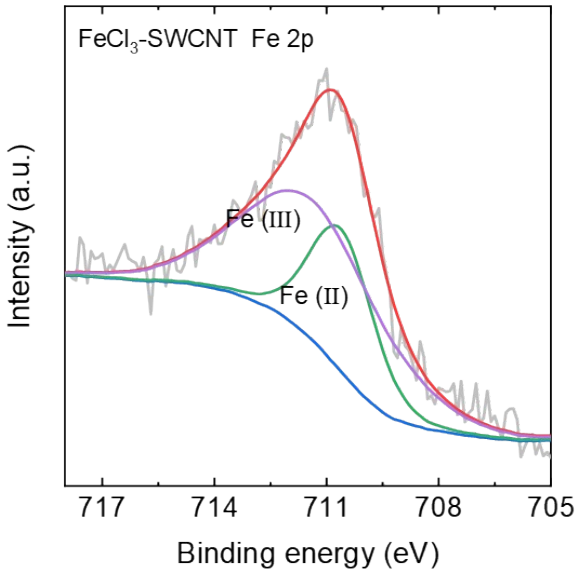

Figure S8. Fe2p spectra of the $FeCl_3$-SWCNT.

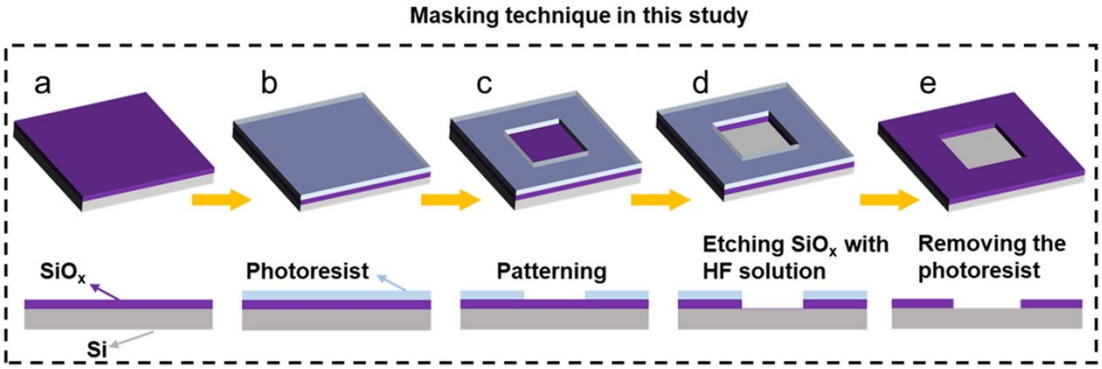

Figure S9. Fabricating the Si substrate with the 3×3 mm^2 active area.

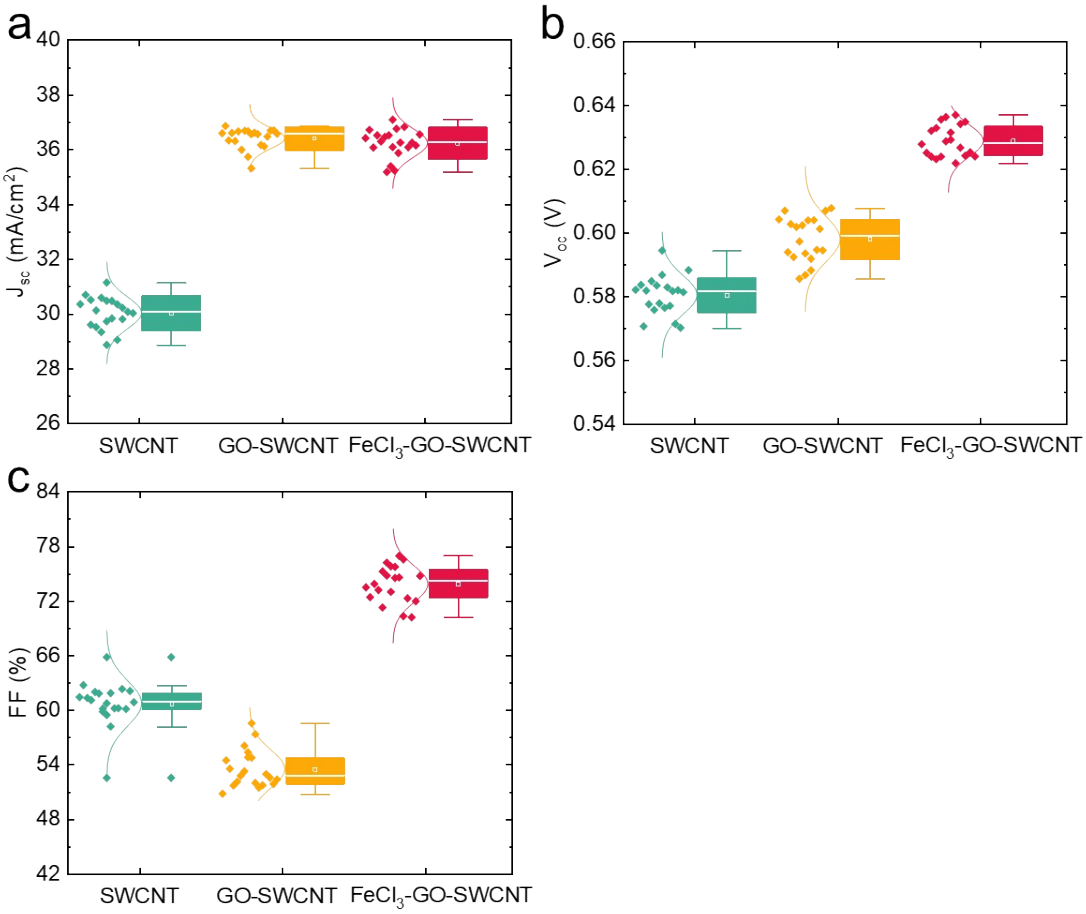

Figure S10 Distributions of the (a) J_{SC}, (b) V_{OC} and (c) FF values for the SWCNT/Si (green), GO-SWCNT/Si (yellow), and $FeCl_3$-GO-SWCNT/Si (pink) solar cells.

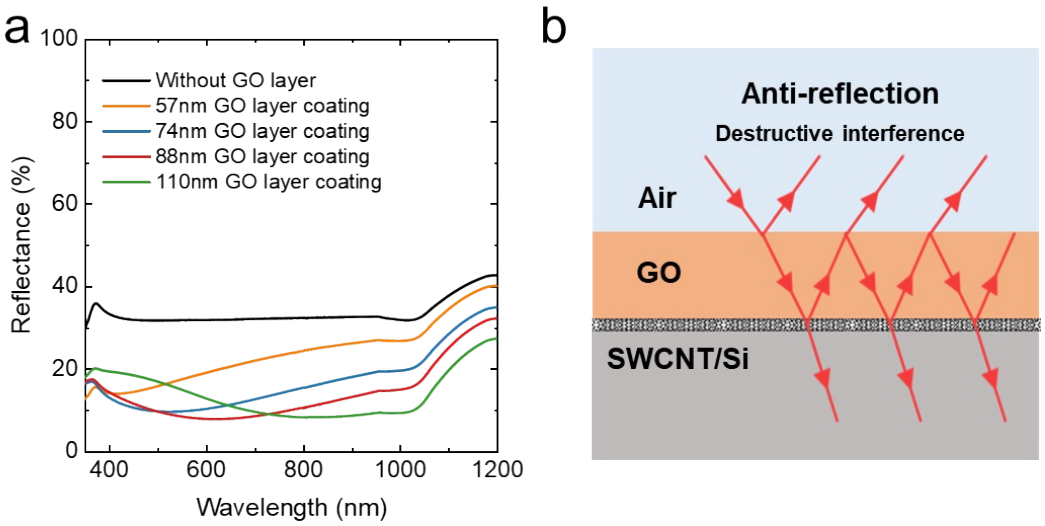

Figure S11. (a) Reflection spectra of GO-SWCNT/Si solar cells with different GO thicknesses. (b) Illustration of the antireflection effect of the GO layer.

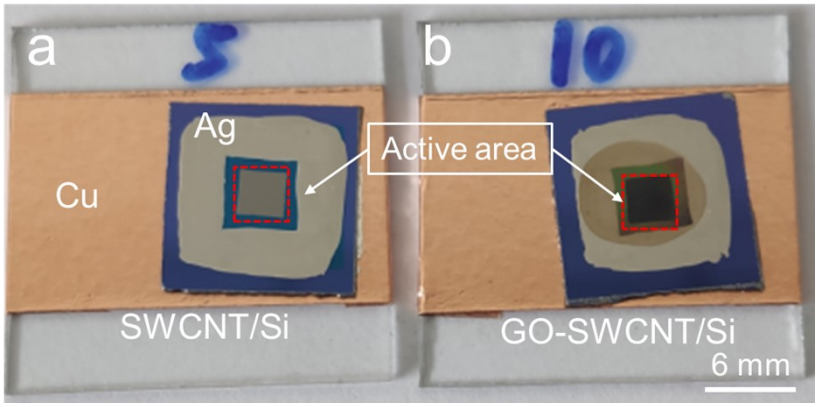

Figure S12 Photograph of the (a) SWCNT/Si and (b) $FeCl_3$-GO-SWCNT/Si solar cells

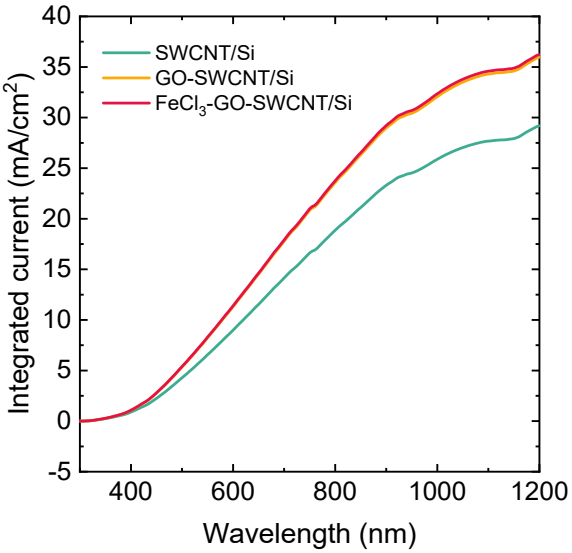

Figure S13 Calculated integrated photocurrent under AM 1.5G irradiation of the SWNCT/Si, GO-SWCNT/Si and $FeCl_3$-GO-SWCNT/Si solar cells

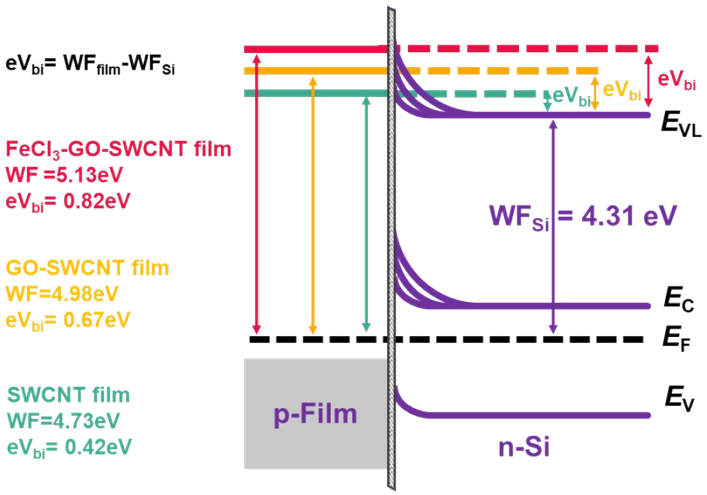

Figure S14. Energy band diagram of the SWCNT/Si (green), GO-SWCNT/Si (orange) and $FeCl_3$-GO-SWCNT/Si (red) solar cells

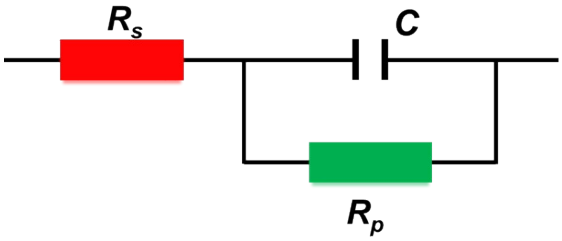

Figure S15. The equivalent circuit for the solar cell.

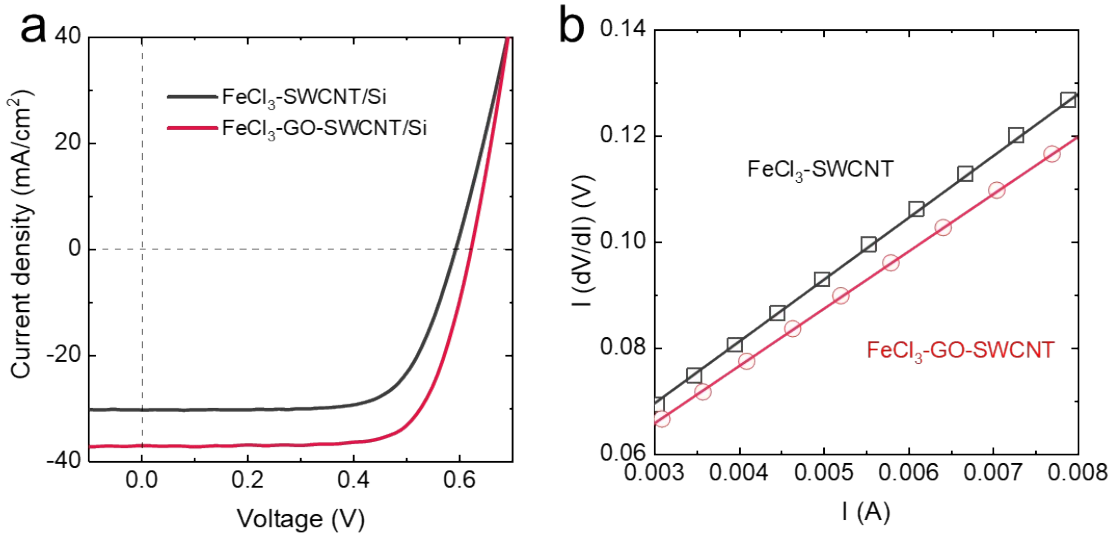

Figure S16. (a) Current density-voltage (J-V) curves and (b) series resistances of the $FeCl_3$-SWCNT/Si and $FeCl_3$-GO-SWCNT/Si solar cells

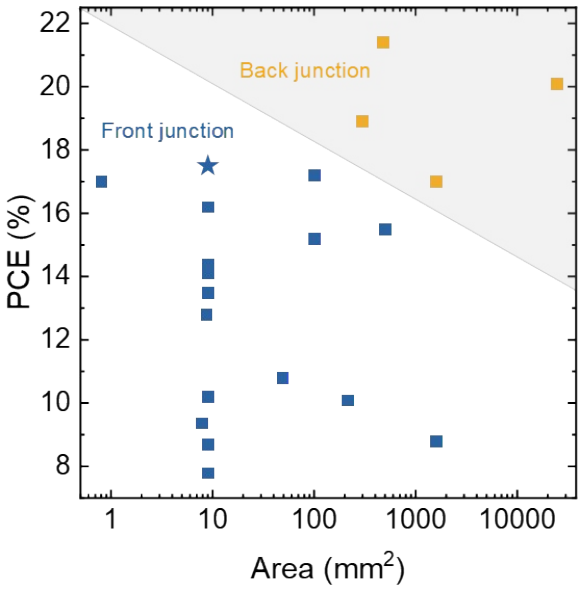

Figure S17. PCE values of representative SWCNT/Si heterojunction solar cells with a front junction (blue) and with a back junction (yellow) [4-18]. The star shows the result achieved in this study.

Table S1 The experimental and standard interspaces of (003) and (006) crystal planes for the $FeCl_3$.

$FeCl_3$	(003)	(006)
Experiment	0.59	0.29
Standard	0.59	0.29

Table S2 The content of carbon-containing functional groups in GO-SWCNT and $FeCl_3$-GO-SWCNT.

Sample	C=C	C-C	C-O	C=O	O-C=O
GO-SWCNT	42.2	8.2	29.4	15.3	4.9
$FeCl_3$-GO-SWCNT	58.1	5.7	22.1	12.2	1.9

Table S3 The Fe(III)/Fe(II) ratio in $FeCl_3$ and $FeCl_3$-GO-SWCNT.

Sample	Fe(III)	Fe(II)	Fe(III)/Fe(II)
$FeCl_3$	73.1±1.7	26.9±1.7	2.73±0.23
$FeCl_3$-GO-SWCNT	53.1±6	46.9±6	1.15±0.28
$FeCl_3$-SWCNT	66.2±1	33.8±1	1.96±0.09

Table S4. Photovoltaic performance of the SWCNT/Si, GO-SWCNT/Si, and $FeCl_3$-GO-SWCNT/Si solar cells under 1 sun (AM 1.5 G, 100 mW cm^{-2})

Sample	J_{SC} (mA/cm^2)	V_{OC} (V)	FF (%)	PCE (%)
SWCNT/Si	**30.6**	**0.581**	**62.3**	**11.1**
	(30.0±0.58)	(0.580±0.006)	(60.7±2.48)	(10.6±0.45)
GO-SWCNT/Si	**36.4**	**0.603**	**56.1**	**12.3**
	(36.4±0.38)	(0.598±0.007)	(54.0±2.09)	(11.7±0.45)
$FeCl_3$-GO-SWCNT/Si	**36.7**	**0.637**	**74.6**	**17.5**
	(36.3±0.51)	(0.629±0.005)	(73.9±2.01)	(16.9±0.46)

Data and statistics are based on twenty cells for each condition. Values in bold are obtained from the best device and the value in brackets is the average value.

Table S5. EIS fitting data of three solar cells over the high-frequency range of 10 Hz to 1 MHz

Sample	R_p (kΩ)	C (nF)	$\tau=R_p*C$ (μs)
SWCNT/Si	30.7	11.45	351.5
GO-SWCNT/Si	27.1	11.45	310.3
$FeCl_3$-GO-SWCNT/Si	41.6	11.76	489.2

Table S6. Photovoltaic performance of the $FeCl_3$-SWCNT/Si and $FeCl_3$-GO-SWCNT/Si solar cells under 1 sun (AM 1.5 G, 100 mW cm^{-2})

Sample	J_{SC} (mA/cm^2)	V_{OC} (V)	FF (%)	PCE (%)	R_S (Ω)	J_0 ($mA\ cm^{-2}$)	Φ (eV)
$FeCl_3$-SWCNT/Si	30.3	0.594	70.9	12.8	11.7	1.03×10^{-4}	0.827
$FeCl_3$-GO-SWCNT/Si	35.2	0.626	77.0	17.0	10	3.77×10^{-5}	0.854

Table S7 PCE values of representative SWCNT/Si heterojunction solar cells

Year	Area (mm^2)	J_{SC} (mA/cm^2)	V_{OC} (V)	PCE (%)	Stability	Optimization methods	Front/Back junction	Ref.
2014	**49**	**31**	**0.51**	**10.8**	**-**	**Chlorosulfonic acid doping + silver nanowires + TiO_2 coating**	**Front**	[4]
2015	**9**	**24.5**	**0.540**	**8.7**	**7 days ~40%**	**$SOCl_2$ doping + polymer interlayer**	**Front**	[5]
2015	**0.8**	**36.6**	**0.59**	**17**	**-**	**MoO_x coating**	**Front**	[6]
2016	**9**	**24.2**	**0.500**	**7.8**	**7 days ~57%**	**$SOCl_2$ doping + polymer coating**	**Front**	[7]
2016	**215**	**25.3**	**0.63**	**10.1**	**2 days**	**HNO_3 doping + TiO_2**	**Front**	[8]

					~90%	coating + CNT strips		
2017	9	26.8	0.610	13.5	-	$SOCl_2$&$AuCl_3$ doping + gold grid	Front	[9]
2017	7.9	26.9	0.540	9.37	12 days ~40%	$SOCl_2$ doping+ Black Phosphorus	Front	[10]
2017	9	36.1	0.540	14.1	Over one year	$CuCl_2$/$Cu(OH)_2$ coating	Front	[11]
2017	9	28.6	0.548	10.2	One day 78%	PEDOT:PSS coating	Front	[12]
2017	8.7	28.3	0.575	12.8	15 days ~75%	$AuCl_3$ doping + spiro-OMeTAD interlayer + gold grid	Front	[13]
2019	9	35.4	0.63	16.2	21 days ~88%	$ZrCl_4$+$FeCl_3$ coating	Front	[14]
2019	100	32.8	0.661	17.2	7 days ~81%	Nafion doping + gold grid + texturing Si	Front	[15]
	500	32.8	0.639	15.5			Front	
2020	9	36.7	0.549	14.4	Over 100 days	Nafion coating	Front	[16]
2020	100	37.5	0.624	15.2	-	Nafion doping + SiNx layer + silver grid + texturing Si	Front	[17]
	1600	34	0.600	8.8	-		Front	
	300	38.8	0.631	18.9	-		Back	
	1600	37	0.638	17	-		Back	
2020	480	39.9	0.654	21.4	-	Nafion doping + SiNx layer + silver grid + texturing Si	Back	[18]
	24571	39.5	0.646	20.1	-		Back	
2021	9	36.7	0.637	17.5	15 days 90%	$FeCl_3$ doping + GO coating	Front	This work

Reference

[1] S. Jiang, P.-X. Hou, M.-L. Chen, B.-W. Wang, D.-M. Sun, D.-M. Tang, Q. Jin, Q.-X. Guo, D.-D. Zhang, J.-H. Du, K.-P. Tai, J. Tan, E. I. Kauppinen, C. Liu, H.-M. Cheng, Sci Adv **2018**, 4, eaap9264.

[2] X.-G. Hu, P.-X. Hou, C. Liu, F. Zhang, G. Liu, H.-M. Cheng, Nano Energy **2018**, 50, 521.

[3] S. Pei, Q. Wei, K. Huang, H.-M. Cheng, W. Ren, Nat. Commun. **2018**, 9, 145.

[4] X. Li, Y. Jung, J.-S. Huang, T. Goh, A. D. Taylor, Adv. Energy. Mater. **2014**, 4, 1400186.

[5] L. Yu, D. D. Tune, C. J. Shearer, J. G. Shapter, ChemNanoMat **2015**, 1, 115.

[6] F. Wang, D. Kozawa, Y. Miyauchi, K. Hiraoka, S. Mouri, Y. Ohno, K. Matsuda, Nat. Commun. **2015**, 6, 1.

[7] L. P. Yu, D. D. Tune, C. J. Shearer, J. G. Shapter, Solar Energy **2015**, 118, 592.

[8] W. Xu, S. Wu, X. Li, M. Zou, L. Yang, Z. Zhang, J. Wei, S. Hu, Y. Li, A. Cao, Adv. Energy. Mater. **2016**, 6, 1600095.

[9] J. M. Harris, R. J. Headrick, M. R. Semler, J. A. Fagan, M. Pasquali, E. K. Hobbie, Nanoscale **2016**, 8, 7969.

[10] M. Bat-Erdene, M. Batmunkh, S. A. Tawfik, M. Fronzi, M. J. Ford, C. J. Shearer, L. Yu, M. Dadkhah, J. R. Gascooke, C. T. Gibson, J. G. Shapter, Adv. Funct. Mater. **2017**, 27, 1704488.

[11] K. Cui, Y. Qian, I. Jeon, A. Anisimov, Y. Matsuo, E. I. Kauppinen, S. Maruyama, Adv. Energy. Mater. **2017**, 7, 1700449.

[12] Q. Fan, Q. Zhang, W. Zhou, X. Xia, F. Yang, N. Zhang, S. Xiao, K. Li, X. Gu, Z. Xiao, H. Chen, Y. Wang, H. Liu, W. Zhou, S. Xie, Nano Energy **2017**, 33, 436.

[13] L. Yu, M. Batmunkh, T. Grace, M. Dadkhah, C. Shearer, J. Shapter, J. Mater. Chem. A **2017**, 5, 8624.

[14] H. Wu, X. Zhao, Y. Sun, L. Yang, M. Zou, H. Zhang, Y. Wu, L. Dai, Y. Shang, A. Cao, Solar RRL **2019**, 3, 1900147.

[15] D. D. Tune, N. Mallik, H. Fornasier, B. S. Flavel, Adv. Energy. Mater. **2020**, 10, 1903261.

[16] Y. Qian, I. Jeon, Y.-L. Ho, C. Lee, S. Jeong, C. Delacou, S. Seo, A. Anisimov, E. I. Kaupinnen, Y. Matsuo, Y. Kang, H.-S. Lee, D. Kim, J.-J. Delaunay, S. Maruyama, Adv. Energy. Mater. **2020**, 10, 1902389.

[17] J. H. Chen, D. D. Tune, K. P. Ge, H. Li, B. S. Flavel, Adv. Funct. Mater. **2020**, 30, 2000484.

[18] J. Chen, L. Wan, H. Li, J. Yan, J. Ma, B. Sun, F. Li, B. S. Flavel, Adv. Funct. Mater. **2020**, 30, 2004476.